Available online at www.sciencedirect.com
ScienceDirect
Geochimica et Cosmochimica Acta 72 (2008) 2377–2391
Geochimica et Cosmochimica Acta
www.elsevier.com/locate/gca

# Age and pyrite Pb-isotopic composition of the giant Sukhoi Log sediment-hosted gold deposit, Russia

Sebastien Meffre [a,*], Ross R. Large [a], Robert Scott [a], Jon Woodhead [b], Zhaoshan Chang [a], Sarah E. Gilbert [a], Leonid V. Danyushevsky [a], Valeriy Maslennikov [c], Janet M. Hergt [b]

[a] *CODES ARC Centre of Excellence in Ore Deposits, University of Tasmania, Private Bag 79, Hobart 7001, Australia*
[b] *School of Earth Science, University of Melbourne, Melbourne 3010, Australia*
[c] *Institute of Mineralogy, Russian Academy of Science, Urals Branch, Miass, Russia*

Received 17 September 2007; accepted in revised form 4 March 2008; available online 13 March 2008

**Abstract**

Sukhoi Log is one of the largest gold deposits in Russia (1100 t Au at 2.45 g/t). Like many other sediment-hosted gold deposits throughout the world, Sukhoi Log preserves textural, structural and geochemical evidence for multiple generations of Au enrichment and pyrite growth.

The deposit is located in the Lena gold province of Siberia, on the edge of the Siberian Craton and occurs in the core of a recumbent anticline in a Neoproterozoic black shale and quartz-rich siltstone–sandstone turbidite succession. Temporal constraints on pyrite paragenesis at the deposit have been determined using laser ablation inductively coupled mass spectrometry (LA-ICPMS) measurements of U, Th and Pb isotopes in pyrite, monazite and zircon. LA-ICPMS age determinations on detrital zircons indicate the host rocks were deposited after $600 \pm 10$ Ma and derived from a mixture of Palaeoproterozoic and Neoproterozoic sources. The U, Th and Pb isotopic systematics indicate the cores of large monazite crystals, which predate obvious tectonic fabric development in the host rocks, began growing at $573 \pm 12$ Ma. The rims of the same monazite crystals formed at $516 \pm 10$ Ma, during peak metamorphism and deformation. Small monazite crystals also grew in the sedimentary rocks during the Devonian ($374 \pm 20$ Ma) and the Carboniferous or Early Permian ($288 \pm 22$ Ma), possibly in response to fluid movements triggered by synchronous granite intrusion in the area. Multi-collector and quadrupole LA-ICPMS Pb isotopic determination on pyrite, combined with overprinting criteria, show that the earliest (stratiform) Pb and Au-bearing pyrite formed prior to metamorphism—possibly during sedimentation or early diagenesis (575–600 Ma). Small Au-rich pyrite nodules preserved as cores to folded bedding-parallel pyrite–quartz veins probably grew during late diagenesis or early metamorphism. Large pyrite euhedra, which overgrow the strong axial planar cleavage in the host rocks, have more radiogenic Pb-isotopic compositions and formed either late during or after deformation. Framboidal pyrite that is overgrown by both the late diagenetic–early metamorphic and syn- to post-metamorphic pyrite has the most radiogenic Pb-isotopic composition suggesting exchange with radiogenic Pb in the matrix may have continued until late in the history of the deposit.

The dating and Pb isotopes support a multistage origin for the gold deposit with Au first introduced during or prior to growth of the earliest stratiform pyrite and progressively re-concentrated (with or without addition of further gold) during later metamorphic events.


* Corresponding author. Fax: +61 3 62262547.
*E-mail address:* smeffre@utas.edu.au (S. Meffre).

0016-7037/$ - see front matter © 2008 Elsevier Ltd. All rights reserved.
doi:10.1016/j.gca.2008.03.005

## 1. INTRODUCTION

Sukhoi Log is a large (1100 t Au) sediment-hosted gold deposit located approximately 500 km to the northeast of Lake Baikal in Russia (Fig. 1). The deposit is hosted in the core of a recumbent antiform in black shale in the upper part of a thick Neoproterozoic sedimentary sequence (Distler et al., 2004; Large et al., 2007) overlying an Early Proterozoic and Archean basement (Fig. 2). The sequence is thought to have been deposited on a long-lived rifted passive margin at the edge of the Siberian Craton (Kuz'min et al., 2006). The host sedimentary sequence is intruded by Palaeozoic granitoids (320–370 Ma). Mineralization is associated with disseminated pyrite and folded bedding-parallel pyrite–quartz veins in the shale, siltstone and sandstone host succession. Previous studies (Distler et al., 2004; Wood and Popov, 2006) summarize the regional geology based on Russian sources, and include descriptions of the mineralogy, fluid inclusions, and stable isotope geochemistry of the deposit. A subsequent study (Large et al., 2007) documents the paragenesis and trace element compositions of multiple pyrite generations at the deposit. Large et al. (2007) identified low-level gold (<5 ppm Au) dissolved in early stratiform arsenian pyrite and higher concentrations of gold (primarily as inclusions of native gold, Au-tellurides and Au-bearing galena) in later generations of coarser grained pyrite. The stratiform pyrite is interpreted to have formed during either sedimentation or early diagenesis, while the coarser grained pyrite formed progressively through late diagenesis, deformation and metamorphism, and post-peak metamorphic hydrothermal alteration. These conclusions a similar to those of a previous study by Buryak (1982), which also argued gold and pyrite deposition spanned the period from sedimentation to metamorphism. In contrast, a recent study on Sukhoi Log (Distler et al., 2004), concludes that the deposit formed long after metamorphism during late Palaeozoic granite intrusion. The early timing for significant gold introduction at Sukhoi Log, proposed by Large et al. (2007), also contrasts with established models for sediment-hosted orogenic gold deposits (e.g. Groves et al., 2003; Goldfarb et al., 2005), in which gold mineralization is generally interpreted to occur late during deformation and metamorphism. The Large et al. (2007) mineralization model for Sukhoi Log is similar in some respects to that proposed by Emsbo et al. (1999, 2006) for the Carlin Au deposits in the USA, where much of the gold is interpreted to have been introduced during sedimentation, and subsequently remobilized and concentrated during later hydrothermal events. This study aims to build on the work of Large et al. (2007) and provide con-

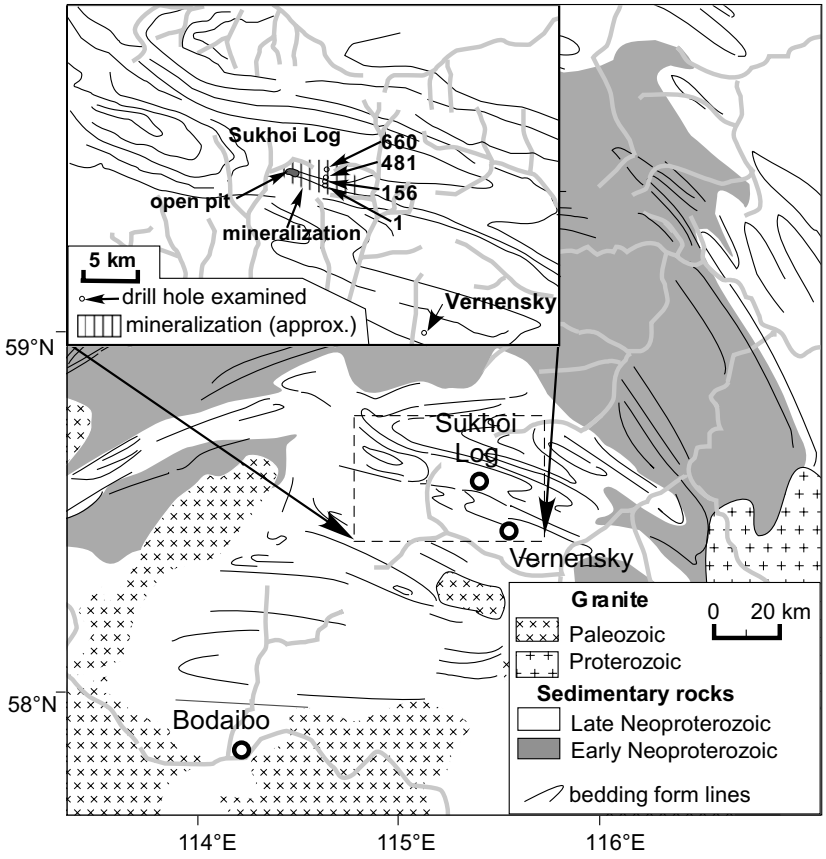


Fig. 1. Regional geological map of the Sukhoi Log district (modified from Large et al., 2007). Lineaments and folds were interpreted from satellite images.

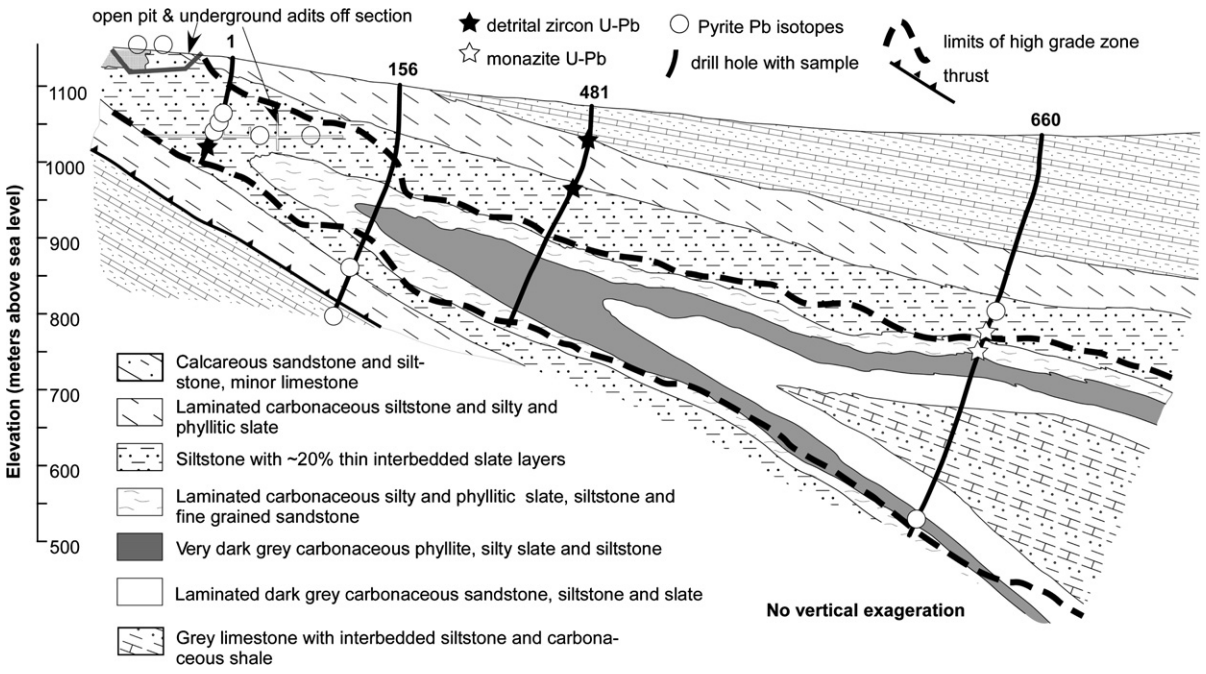


Fig. 2. Cross section of drill holes showing ore zone and samples analysed (modified from Wood and Popov, 2006).

straints on the timing of mineralization. The following approaches were used:

(1) U–Pb dating of detrital zircons in the host rocks to constrain the maximum age for the deposit. Previous constraints on the age of the host rocks are poor. Distler et al. (2004), Wood and Popov (2006) and Kuz'min et al. (2006) report an 800 Ma age (Riphean) for the host strata supported by Pb–Pb dating of carbonates (Fefelov et al., 2000).
(2) U, Th, Pb dating of pre-, syn- and post-metamorphic monazite (e.g. Distler et al., 2004) to improve constraints on the timing of deformation and metamorphism. Previous studies variously state peak metamorphism at Sukhoi Log occurred at $516 \pm 22$ Ma (Distler et al., 2004) and 550–650 Ma (Wood and Popov, 2006), but little information about the minerals and techniques used to determine these ages is presented.
(3) Investigating the Pb isotopic systematics of the different pyrite generations recognised by Large et al. (2007). Pb-isotopic data aids correlation of pyrite types where direct paragenetic constraints are absent (e.g. samples from different parts of the deposit), and can provide a rough indication of the age of pyrite formation based on the model Pb growth curve (e.g. Stacey and Kramers, 1975). Previous Pb isotope studies show Pb at Sukhoi Log plots on the Stacey and Kramers (1975) crustal growth curve at 380–400 Ma (Larin et al., 1997; Distler et al., 2004). In this study we show that the different generations of pyrite at Sukhoi Log also have distinct Pb isotopic signatures.

### 1.1. Pyrite development at Sukhoi Log

Large et al. (2007) recognised a complex but apparently consistent pyrite paragenesis throughout the Sukhoi Log deposit and surrounding host rocks. The earliest pyrite recognised (termed py1 by Large et al., 2007) occurs either in stratiform bands of very fine-grained pyrite or as more patchily developed very fine-grained 'sooty' and framboidal pyrite. In detail, the stratiform bands of fine-grained pyrite are formed by more irregular aggregates of densely clustered 3–7 μm anhedral to subhedral pyrite crystals, crudely aligned parallel to bedding. The stratiform pyrite is folded and overprinted by the axial planar cleavage in the host rocks, and the constituent pyrite aggregates are locally deformed into alignment with the cleavage. Large et al. (2007) interpret these features to indicate the pyrite formed prior to significant grain-scale deformation in the host rocks, probably during sedimentation or early diagenesis. The fine-grained stratiform pyrite contains relatively low levels of arsenic (mostly <1000 ppm As) and up to several ppm Au (see Electronic annex). This type of pyrite is extensively developed through part of the section intersected in drill hole 1, with the pyrite locally forming up to 40% of the rock (Fig. 2) but was not identified in any of the other drill holes sampled by Large et al. (2007). However, framboidal pyrite and isolated clusters of fine-grained 'sooty' pyrite (similar in appearance to that comprising the bands of stratiform pyrite) are widespread throughout the deposit and surrounding host rocks. Although termed py1 by Large et al. (2007), the framboidal pyrite and isolated clusters of sooty pyrite are notably higher in gold (up to 15 ppm Au) and arsenic (0.1–1% As) compared to

the fine-grained stratiform pyrite (see Electronic annex), and as will be shown here, also have distinctly more radiogenic Pb-isotopic signatures. Regardless of these compositional differences, all of the fine-grained pyrite classified as py1 by Large et al. (2007) is overgrown and/or replaced by coarser grained pyrite types where they are developed in the same samples. Accordingly, a broadly similar, early-stage timing for most of the fine-grained pyrite at Sukhoi Log is likely.

Overgrowth relationships, internal textural features and compositional characteristics of the later, coarser grained pyrite provide important constraints on the temporal relationships between ongoing pyrite development, gold mineralization and deformation at Sukhoi Log. Large et al. (2007) distinguished two main types of coarser grained, locally gold-rich pyrite. The earliest coarse-grained pyrite (termed py3 by Large et al., 2007) occurs as isolated subhedral to anhedral (and rarely euhedral) grains or grain clusters and contains minor randomly oriented wall rock mineral inclusions as well as minor to locally abundant inclusions of chalcopyrite, pyrrhotite, sphalerite, galena, arsenopyrite and gold. This type of pyrite is locally overgrown by or included in later coarse-grained euhedral pyrite, which principally occurs as isolated euhedra 0.2–3 cm in size. This latter pyrite type (termed py4 by Large et al., 2007) is the first to record the presence of a well developed axial planar cleavage in the host rocks (preserved as abundant closely spaced, cleavage-parallel trains of very fine-grained, wall rock mineral inclusions within the pyrite euhedra). Py4 also contains inclusions of native gold, gold-tellurides or gold-bearing galena locally, but overall these appear less abundant than in the Py3, which is interpreted to have formed prior to significant cleavage development (Large et al., 2007).

There is generally little variation in the intensity and orientation of cleavage in the wall rocks adjacent to the pyrite euhedra indicating growth late during or after development of the cleavage. However, locally small quartz ± carbonate-filled strain fringes, which parallel the cleavage in the surrounding rock are developed at their edges, and some euhedra have narrow relatively inclusion-free pyrite rims which are interpreted to result from partial overgrowth of the strain fringes. These features provide unambiguous evidence of growth late during fold and cleavage development. Pyrite euhedra which overgrow the cleavage but either lack obvious strain fringes, or have strain fringes that record extension oblique to the axial planar cleavage are also developed locally and may be younger than some of the pyrite classified as Py4 by Large et al. (2007).

The core of the Sukhoi Log deposit, along the axial zone of the recumbent anticline, is characterised by numerous strongly-deformed, discontinuous, predominantly bedding-parallel pyrite–quartz veins (Distler et al., 2004; Wood and Popov, 2006; Large et al., 2007). Similar veins occur elsewhere (e.g. up to 300 m below the main mineralised zone) but they are most abundant in the hinge zone of the anticline. Despite their vein-like appearance, Large et al. (2007) demonstrated these features resulted from multi-stage overgrowths on original bedding-parallel trains of pre-cleavage pyrite nodules, which are preserved as irregular cores in the coarse-grained pyrite forming the veins. These cores contain randomly oriented wall rock mineral inclusions and locally inclusions of chalcopyrite, pyrrhotite, sphalerite, galena, arsenopyrite and gold, and are thus similar in composition and appearance to py3 in the surrounding wall rocks. The nodular cores are enveloped either by pyrite similar to py4 in the wall rocks, which overgrew and preserved the axial planar cleavage, and/or later euhedral relatively inclusion-free pyrite. Originally fibrous quartz strain fringes, which record cleavage-parallel extension, envelope but largely post-date the pyrite (Large et al., 2007). The lack of wall rock inclusions in the outermost parts of the vein pyrite grains may indicate these formed by replacement of the adjacent quartz strain fringe. Large et al. (2007) interpret the lack of a clearly preserved cleavage fabric in the nodular cores to the pyrite veins as evidence these, which are generally the most gold-rich parts of the pyrite, formed prior to cleavage development in the host rocks. Rare inclusions of native gold also occur in the surrounding cleavage-bearing pyrite overgrowth, but gold only occurs along fractures in the outermost inclusion-free pyrite (Large et al., 2007). The quartz strain fringes on the vein pyrite in the core of the deposit are generally much better developed than those adjacent to isolated pyrite euhedra around the periphery, suggesting that either (i) most of the vein pyrite (not just the nodular cores) formed before the isolated pyrite euhedra in the wall rocks, or (ii) more intense deformation occurred along the axial zone of the fold.

Overall, py3 (which forms the earliest phase of relatively coarse-grained pyrite in the wall rocks and the nodular pyrite cores to the bedding-parallel pyrite veins) appears to be the most gold-rich and probably constitutes the bulk of Sukhoi Log ore. This type of pyrite locally contains up to 2% As and commonly less than 2.5 ppm Au in solid solution in addition to inclusions of arsenopyrite and gold. The high arsenic content of the pyrite (see Electronic annex), and associated mineral inclusions (i.e. arsenopyrite, pyrrhotite, chalcopyrite, sphalerite, galena) may suggest a moderate to high temperature hydrothermal origin. However, based on the textural, compositional and overprinting relations documented by Large et al. (2007), both initial gold enrichment and the main stage of gold introduction (and/or incorporation into pyrite) at Sukhoi Log appears to predate significant grain-scale deformation (i.e. cleavage development) in the host rocks.

## 2. METHODS

The analytical work reported in this paper was conducted using the quadrupole and multi-collector ICPMS at the University of Tasmania and the University of Melbourne, respectively. Analyses on both instruments were conducted using both laser and solution modes. Analytical techniques are summarized below.

### 2.1. Zircon geochronology

Zircons were separated by crushing the sample in a ring mill to fit through a 400-μm sieve and panned to concentrate heavy minerals. Magnetic minerals were removed using a hand magnet. As the Sukhoi Log heavy mineral concentrates were dominated by pyrite with relatively rare zircons, individual zircons were hand picked under cross-polarized transmitted light using a single hair on a paint brush. The zircons were then mounted on double sided sticky tape, and epoxy was added to make a 25 mm block. After grinding and polishing to expose the top of the crystals, they were analysed using the LA-ICPMS. The first batch of zircons were analysed using a 213 nm New Wave solid-state laser attached to a Hewlett Packard 4500 quadrupole ICPMS. The zircons were ablated in an He atmosphere in a custom-made chamber with the laser pulsing at 5 Hz and a 30-μm beam diameter delivering approximately 12 J $cm^{-2}$ and drilling at approximately 1 μm $s^{-1}$. The second batch were analysed using a 193 nm solid-state laser (New Wave) and an Agilent 7500cs ICPMS, using similar parameters to the first batch although with a lower laser energy (5 J $cm^{-2}$).

A total of 10 masses were counted ($^{96}Zr$, $^{146}Nd$, $^{193}Hf$, $^{202}Hg$, $^{204}Pb$, $^{206}Pb$, $^{207}Pb$, $^{208}Pb$, $^{232}Th$, $^{238}U$) with longer counting times for Pb isotopes, giving a total quadrupole cycling rate of 0.14 s. Each analysis began with a 30 s analysis of background gas, followed by 30 s with the laser switched on. Four primary (Temora zircons of Black et al., 2003) and two secondary standards (91500 zircons of Wiedenbeck et al., 1995) were analysed before and after each 12 zircons to correct for mass bias, machine drift and down hole fractionation. The concentration of various major and trace elements in the zircons was calculated by assuming stoichiometric Zr and the 91500 standard zircons to correct for mass bias. More details on these methods are provided in Kosler and Sylvester (2003), Black et al. (2004), Jackson et al. (2004) and Meffre et al. (2007).

### 2.2. Monazite geochronology

Monazite is not routinely analysed on the ICPMS, although some preliminary studies have shown that the method can be used (Machado and Gauthier, 1996; Foster et al., 2002). Most igneous and metamorphic monazites are analysed using the electron microprobe (Montel et al., 1996; Berry et al., 2007) because it offers an inexpensive yet accurate method of determining age. However, low temperature monazites such as those from Sukhoi Log, and hydrothermal monazites, are generally too low in Th and U for analysis and can contain significant common Pb (Schandl and Gorton, 2004) resulting in anomalously old ages being obtained from electron probe analyses. The Sukhoi Log monazites were initially analysed on the electron microprobe, but as the Th contents were low, the crystals were re-analysed using the laser ICPMS.

The monazites were analysed in a 2.5 mm polished block of black shale, using similar analytical conditions to those of the zircons described above, but with an 8 μm spot size, due to the high concentration of Th and U in monazites compared to zircons. The RGL4B monazite of Rubatto et al. (2001) were used as a primary standard and monazites from the Hartz Range (Sample 94-222) described by Hand et al. (1999) as a secondary standard.

To better constrain the complex element and isotopic zonation in the crystals, the monazites were also analysed along 10 μm wide line traverses. To correct for mass bias, we first fully characterised the trace elements of the standard monazites (RGL4B monazite of Rubatto et al., 2001) using the electron microprobe, and then analysed the 10 μm line traverses with the LA-ICPMS, using $^{31}P$ as the internal standard element. This gave satisfactory results for most elements, except those with concentrations too low to be analysed precisely on the electron microprobe (Eu, Tm, Ho and Lu). For these elements the mass bias was derived from analyses on the standard glass NIST 612.

### 2.3. Pb isotopes in pyrite

Samples of pyritic black shale were selected from those described by Large et al. (2007) both from Sukhoi Log and from the nearby Vernensky deposit (Figs. 1 and 2). The 2.5 cm round polished blocks made for the earlier pyrite study (Large et al., 2007) were re-analysed for Pb isotopes, concentrating mainly on pyrite samples containing >20 ppm Pb.

Pb isotopes in pyrite were determined using both the Agilent quadrupole instrument at the University of Tasmania described in Section 2.1 and a Nu Plasma multi-collector instrument at the University of Melbourne. We used the quadrupole instrument and the 213 nm solid-state laser to obtain initial Pb isotopic ratios, and then checked some analyses with the multi-collector instrument equipped with a 193 nm excimer gas laser. Accuracy of the different methods used was also checked using an in-house secondary pyrite Pb isotope standard (pyrite 700380). This standard was initially analysed by the Tl-doping solution multi-collector method described in Woodhead (2002) and then analysed by using the laser on both the multi-collector and quadrupole. In general, for high Pb pyrite (>100 ppm), the multi-collector instrument produced higher-precision data than the quadrupole, but was less versatile, as its configuration does not allow for simultaneous measurement of Pb, U and Th. For pyrite with Pb between 50 and 100 ppm the two machines obtained similar levels of precision on individual spots. For pyrite with 20–50 ppm we preferred to use the quadrupole instrument since it was not possible to obtain useful results below 20 ppm with Faraday cup detection on the MC-ICPMS. $^{204}Hg$ interferes with the measurement of $^{204}Pb$ at low concentrations, and high Hg in the blank gas has been a problem reported by most laser-based ICPMS laboratories (Compston, 1999; Kosler and Sylvester, 2003). At the University of Tasmania we have reduced the Hg background by changing the plastic tubing and glass top of our ablation chamber. When all new materials are used the $^{202}Hg$ background decreases below 100 counts per second (cps) and gradually builds up to around 450 cps over time. On both machines the isobaric interference was corrected by measuring $^{202}Hg$. However, this correction adds large uncertainties to the $^{204}Pb$ based ratios

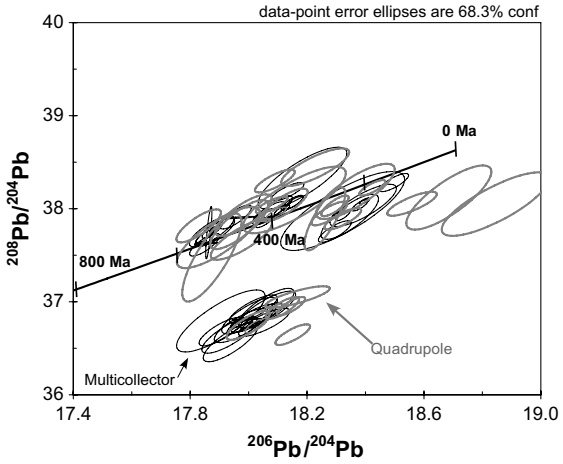


Fig. 3. $^{208}Pb/^{204}Pb$ and $^{206}Pb/^{204}Pb$ diagram comparing precision of the quadrupole and multi-collector laser ablation ICPMS on Sukhoi Log pyrite. The model Pb curve is from Stacey and Kramers (1975). Each ellipse for the quadrupole data is the pooled average of 4–8 spots on the same pyrite type within a single sample. Multi-collector data are individual spot analyses.

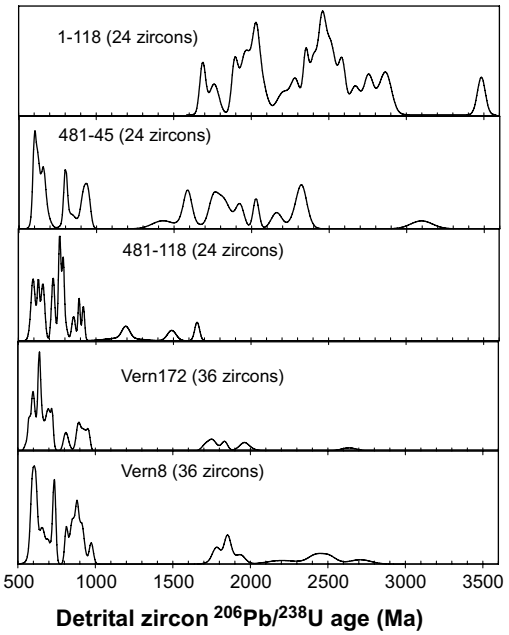


Fig. 4. Probability plot $^{206}Pb/^{238}U$ ages of detrital zircons from the Sukhoi Log and Vernensky deposit. Each of the plots are histograms but instead of showing the ages plotted as a bar graph with discrete bins for different age zircons, the ages and their errors are plotted as a continuous probability function. This has the advantage of taking both the ages and their errors into account.

when $^{204}Pb$ is low. The lower precision data obtained on the quadrupole were to some extent compensated for by pooling spots from similar pyrite, ensuring that the mean square weighted deviations on the weighted average remained below 2 (using the Isoplot software of Ludwig, 2003). On the quadrupole instrument the spot size was partially determined by the size of the pyrite, but also the count rate on $^{208}Pb$ which should be maintained between 40,000 and 5 million cps. Below this range the data is not useful, due to poor precision on $^{204}Pb$, above this the detector becomes saturated and the concentrations are no longer directly proportional to the count rate. On the multi-collector with the Faraday cup detectors this is not an issue, so the largest possible spot size was used. Overall the two systems provided similar and complementary results showing that the Pb isotopic analysis on both multi-collector and quadrupole instruments is reliable and can be widely applied (Fig. 3).

## 3. RESULTS

### 3.1. Maximum age of the host sequence

All 144 detrital zircons analysed from five siltstone and sandstone samples of the host sequence (3 from Sukhoi Log and 2 from Vernensky), are Precambrian in age (see Electronic annex for age of individual zircons and zircon standards analysed at the same time). Two groups of zircons are present; one Neoproterozoic, dominated by euhedral zircons, the other Archean, dominated by dark pink-brown round zircons. Different samples show different proportions of these two groups, indicating a variable degree of mixing between Neoproterozoic and Archean zircon sources during sedimentation (Fig. 4). Samples from the nearby Vernensky deposit (20 km SW, Fig. 1) are dominated by the younger zircons.

The youngest detrital zircons from both areas unequivocally show that the host sedimentary sequence is much younger than previously reported. Four of the five analysed samples have zircons that are between 600 and 700 Ma, and the weighted average age of the youngest zircons from those samples is 600 ± 10 Ma (2 sigma) (Fig. 5). This age is close to the metamorphic and diagenetic ages for monazites (see below) indicating that although these are mostly continental-derived siliciclastics rocks, there was also a significant juvenile (i.e. syn-sedimentary) felsic volcanic input into the basin.

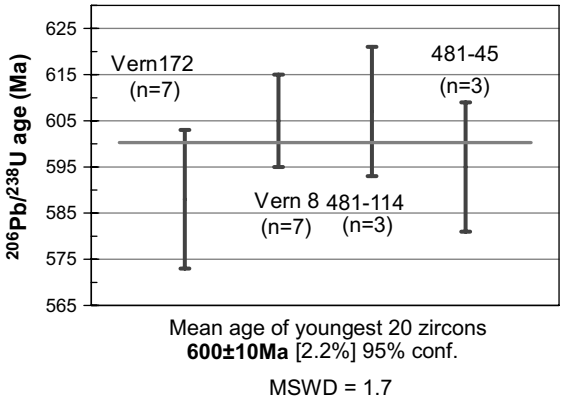


Fig. 5. Plot showing the $^{206}Pb/^{238}U$ weighted average age and precision of the youngest zircons in 4 of the 5 samples analysed. Error bars are 2 standard error, $n$ = number of young zircon pooled from each samples.

An older darker zircon population, mostly between 1500 and 2800 Ma, also occurs in these rocks. These are most likely derived from either Early Proterozoic and Neo-Archean granitoids reported from the area (Larin et al., 1997) or from the Siberian Craton.

### 3.2. Age of diagenesis and metamorphism

Large irregular crystals of monazite (150–250 μm) at Sukhoi Log were first reported by Distler et al. (2004) in sedimentary rocks. These monazite crystals are much larger than the grainsize of the rocks (30–80 μm, Fig. 6A) and therefore must have grown *in situ* after sedimentary deposition. The foliation also tends to wrap around the crystals suggesting they began forming early during or prior to deformation and metamorphism. The two large monazite crystals from drill hole 660 (Fig. 2), which were selected for detailed investigations, exhibit strong compositional zonation with high Th (up to 3 %) on the edge of the crystals and low Th (0.1–0.3%) in the centres (Fig. 6B and C). Uranium shows the opposite distribution with high U in the centre and lower U in the high Th rims (Fig. 6C). The $^{206}Pb/^{238}U$ systematics indicate that the older central parts of the monazite crystals began growing in the Neoproterozoic (weighted average $^{207}Pb$ corrected $^{206}Pb/^{238}U$ age $573 \pm 12$ Ma), 5–50 m.y. after deposition of the host rocks based on the age of the youngest detrital zircons. Common Pb correction is necessary as the monazites are discordant on concordia diagrams with regressions indicating contamination by common Pb (Fig. 7).

The $516 \pm 10$ Ma $^{207}Pb$ corrected $^{208}Pb/^{232}Th$ isotopic age on the high Th low U monazite rims is significantly younger than the cores suggesting that the rims formed 35–80 m.y. after the cores. This age difference is interpreted

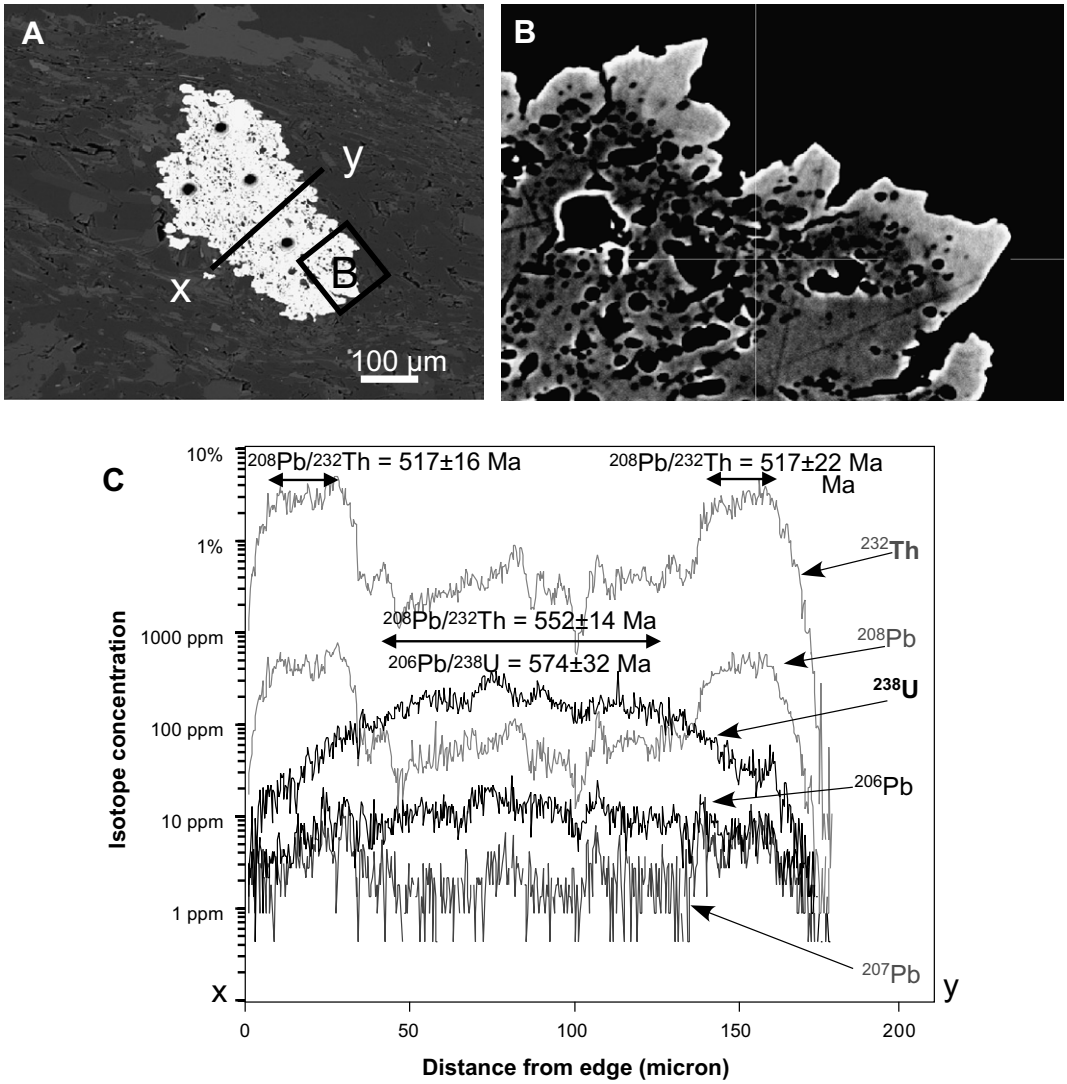


Fig. 6. Chemistry and age of large monazites. (A) Backscattered electron image of large monazite showing the shape and size of the crystal (circular holes are laser ablation pits) The *x*–*y* line represents the position of a laser ablation traverses shown in (C). (B) Detail of backscattered image showing high Th rim (bright rim of crystal). Note: the bright edge is not an edge effect as the bright edge disappears where the edge of the monazite penetrates into the low Th zone. (C) Laser ablation traverse across crystal showing the distribution of U, Th and Pb isotopes. Radiometric ages are quoted at 95% confidence.

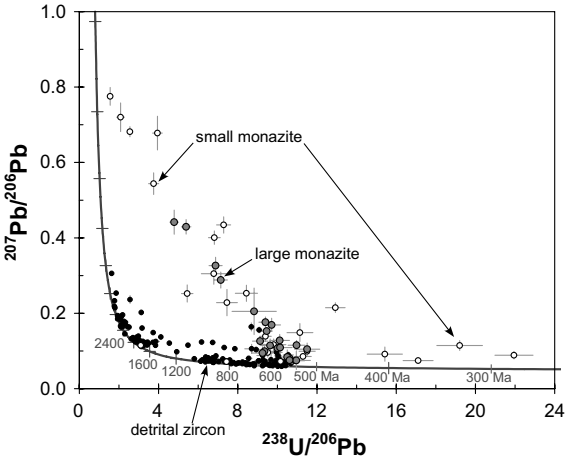


Fig. 7. Reverse concordia plot of U and Pb isotopic composition of zircons and monazite. Open circles are small monazite, grey circles are large monazites and black circles are zircons. Error crosses are 1 standard error.

to reflect successive episodes of monazite growth rather than Pb loss from the rims of the crystals. Episodic monazite growth during low grade metamorphism has been reported from other mudstone and schist sequences throughout the world (see review by Foster et al., 2002).

In the older cores, the $^{206}Pb/^{238}U$ ages are slightly older that the $^{208}Pb/^{232}Th$ ages. At first this was considered to be an analytical problem, but this was discounted when the same results were obtained using a different Laser and different ICPMS. Rather, the discrepancy between the two decay systems is most likely due to partial resetting of the monazite during metamorphism. During diagenesis, low Th REE phosphates were formed in the samples (either low Th monazite or hydrated REE phosphate such as florencite). Thirty-five to 80 m.y. later, when the outer rim of higher Th monazite was formed, it is possible that the low Th core was secondarily enriched in Th without fully removing the radiogenic Pb that had already accumulated in the structure. This mechanism could account for the age discrepancy. The isotopic systematics therefore suggest that the monazite began growing at 573 Ma prior to cleavage development and grew a high Th rim at around 516 Ma, syn- to post-cleavage development. The 516 Ma age determined for the monazite rims is identical to that previously reported for peak metamorphism and deformation in the area (Distler et al., 2004).

Despite their different U and Th contents the large monazite core and rim have similar chondrite normalised REE contents characterised by very low heavy REE (Fig. 8). Low heavy REE contents in monazite is a feature of crystals which have grown under low temperature conditions (chlorite zone, <350 °C Heinrich et al., 1997), in contrast with higher temperature monazite, which tend to have much higher REE contents (e.g. the central Australian monazite which we used as our age standard shown in Fig. 8).

Smaller monazite crystals were also analysed from various levels in drill hole 660 and from a sample in the underground workings (see Electronic annex). These included two small (10 μm) high Th detrital monazite crystals which yielded Early and Middle Proterozoic ages, and numerous lower Th monazite crystals which occur as inclusions in both pyrite and the shale matrix. The U–Pb ages from most of these inclusions (40 analyses) are compatible with growth between 500 and 600 Ma but five of the crystals have significantly younger ages suggesting further monazite growth at $374 \pm 20$ and $288 \pm 22$ Ma (Fig. 9). These younger ages are close to those reported for large granite intrusions 75 km to the south of Sukhoi Log and the small Konstantinovsky granite stock 6 km south-west of the deposit (i.e. 350 and 290 Ma, Larin et al., 1997; Kuz'min et al., 2006). All of the monazite data discussed here is presented in Electronic annex.

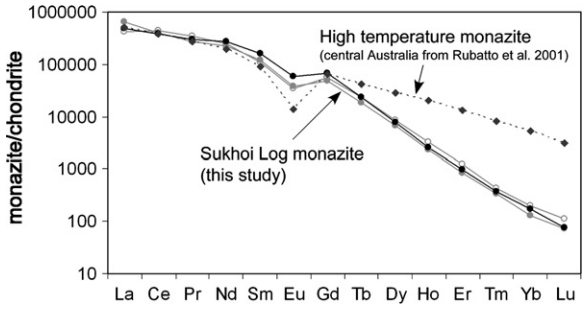


Fig. 8. Monazite rare earth element chondrite normalised plots showing the depletion of heavy REE compared to higher temperature monazites. Normalization values from Sun and McDonough (1989).

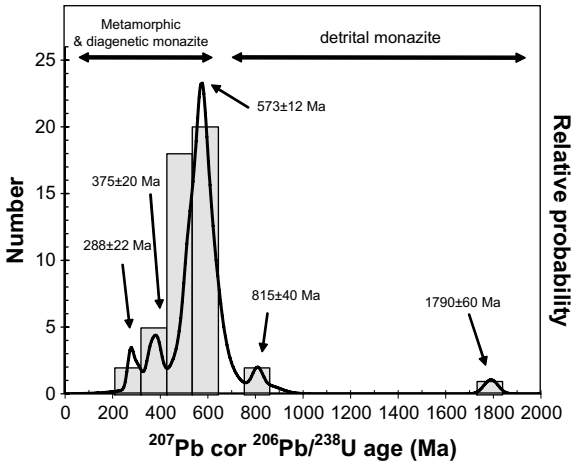


Fig. 9. Histogram showing all of the $^{207}Pb$ corrected $^{206}Pb/^{238}U$ LA-ICPMS monazite data from the Sukhoi shales. Note that the high Th large monazite rims are not included as they have very low U and very large uncertainties.

### 3.3. Pb isotopes in pyrite

The Pb-isotopic compositions of 350 individual pyrite crystals were analysed in 32 samples (Fig. 10). Data from the quadrupole instrument are pooled to make the dia-

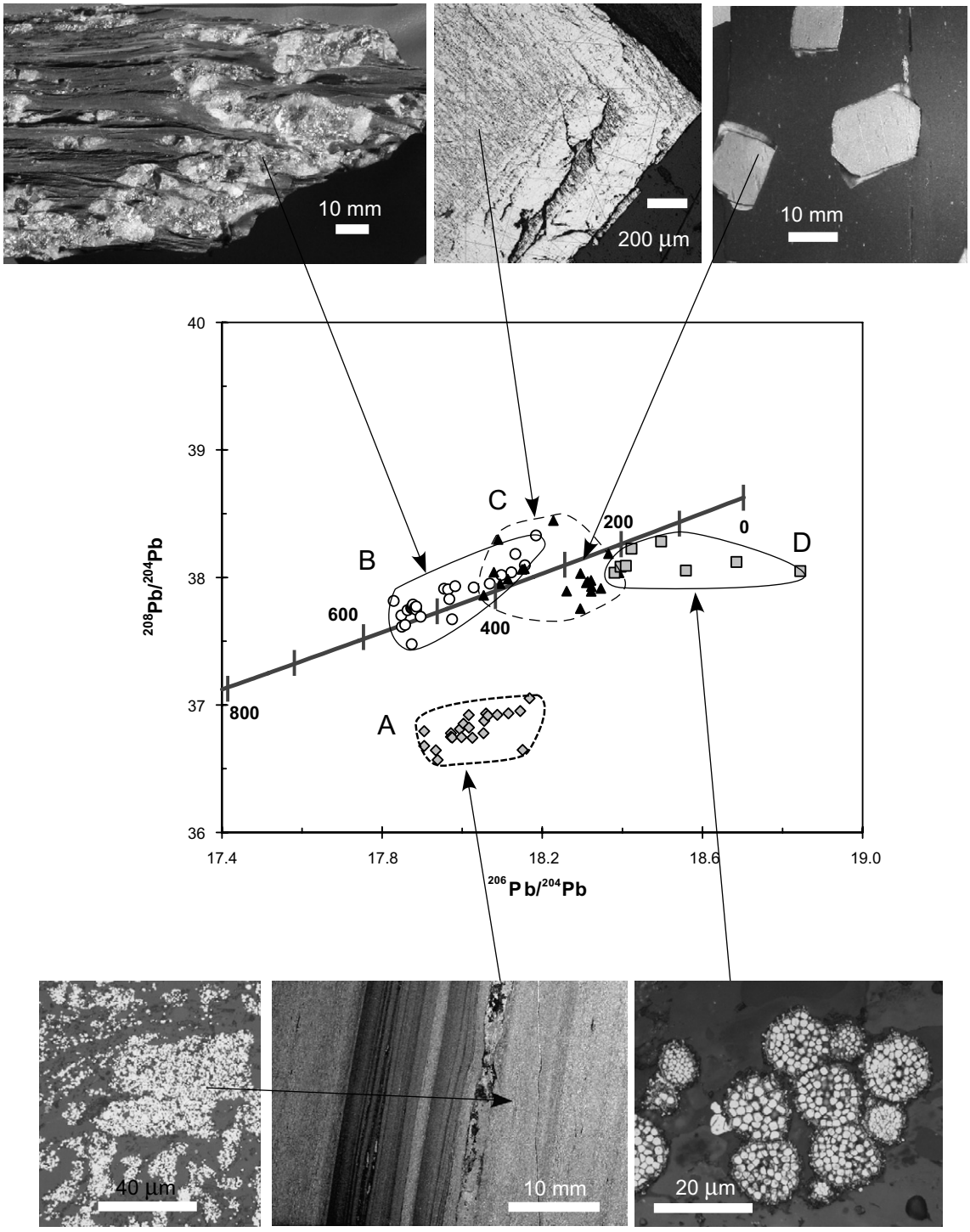


Fig. 10. Laser ablation ICPMS analyses of $^{208}Pb/^{204}Pb$ and $^{206}Pb/^{204}Pb$ in pyrite from the Sukhoi Log deposit. The model Pb curve is from Stacey and Kramers (1975). The field labelled A (diamonds) shows Pb-isotopic composition of the early stratiform pyrite, field labelled B (circles) contains data from cores of early folded veins, field labelled C (triangles) contains data from large euhedral pyrite and field labelled D (squares) contains small framboidal and sooty pyrite with more radiogenic Pb-isotopic composition.

grams less confusing and to improve precision on individual pyrite types. The weighted average data represent analyses of a single pyrite type in single 25 mm polished mount for which the mean square weighted deviations (MSWD) is $<2$ (but usually $<1.3$). Data from the multi-collector ICPMS are presented as points for individual analyses.

The Pb isotope data for Sukhoi Log pyrite shows a range of composition similar to that previously reported

for the Lena gold province (Larin et al., 1997) (Fig. 10). However, the data show that specific pyrite types have restricted Pb-isotopic compositions that appear to place broad temporal constraints on pyrite growth. The Pb-isotopic data can be subdivided into 4 main groups (labelled A–D in Fig. 10) based on pyrite textural features and overprinting criteria:

A. The early fine-grained stratiform pyrite (in part py1 of Large et al., 2007) has unusually low $^{208}Pb/^{204}Pb$ but plot between 500 and 600 Ma on the crustal $^{207}Pb/^{204}Pb$ versus $^{206}Pb/^{204}Pb$ growth curve of Stacey and Kramers (1975). They generally contain between 0.3 and 1.2 ppm Au and relatively high Pb.
B. The locally gold inclusion-rich nodular cores to pyrite crystals from folded pyrite–quartz veins plot on the growth curve on both $^{208}Pb/^{204}Pb$ and $^{207}Pb/^{204}Pb$ versus $^{206}Pb/^{204}Pb$ diagrams. The cores are enveloped by later stage pyrite which contains so little Pb that we were unable to analyse them using the laser. The cores of the pyrite crystal contain many small inclusions, including numerous small galena crystals (1–3 μm), which are the main source of the Pb.
C. Large subhedral to euhedral pyrites (py4 of Large et al., 2007) which show textural evidence of growth either late during or after deformation plot on the growth curve with a more radiogenic signature, at 200–450 Ma, on both $^{208}Pb/^{204}Pb$ and $^{207}Pb/^{204}Pb$ versus $^{206}Pb/^{204}Pb$ diagrams.
D. Patchily developed framboidal pyrite and very fine-grained "sooty" pyrite with relatively high Au, Pb and As forms a distinct group with more radiogenic Pb than any of the other pyrite at Sukhoi Log. In Large et al. (2007) this pyrite (described as py1 and py2) was grouped with the stratiform py1 (i.e. Group A, above), based on gross similarities in texture, trace element composition and overprinting relations relative to later coarser grained pyrite types. However, based on their very radiogenic Pb compositions and notably higher As and Au contents (see Electronic annex) the framboidal pyrite and isolated clusters of fine-grained 'sooty' pyrite are separated from the fine-grained stratiform pyrite (Group A) in this paper.

The Pb isotope data are presented in the Electronic annex.

## 4. DISCUSSION

### 4.1. Pb sources

The Pb isotopes in pyrite from Sukhoi Log are broadly compatible with the trace element and paragenetic observations of Large et al. (2007) supporting a protracted multi-stage history of pyrite formation and gold mineralization at Sukhoi Log. Textural and Pb-isotopic evidence suggest the earliest auriferous pyrite probably formed during diagenesis, before significant deformation and metamorphism of the host succession. The earliest pyrite (Group A on Fig. 10) contains Pb derived from a source with a distinctive low $^{208}Pb/^{204}Pb$ ratio. Later pyrite types (Groups B, C and D) plot close to the average crustal growth curve (Fig. 10) suggesting Pb was subsequently derived from a well-mixed crustal Pb source.

The low $^{208}Pb/^{204}Pb$ ratios for the early stratiform pyrite are unusual because they do not coincide with any of the known Pb isotopic reservoirs. Although the stratiform pyrite has the highest U/Pb ratios of any of the pyrite analysed at Sukhoi Log, its distinctive Pb-isotopic composition is unlikely to be the result of *in situ* decay of U and Th since pyrite growth. Correction for *in situ* decay of U and Th in the pyrite since 600 Ma only slightly shifts the $^{206}Pb/^{204}Pb$ ratio of the pyrite (Figs. 11 and 12) and causes no appreciable shifts to the $^{207}Pb/^{204}Pb$ and $^{208}Pb/^{204}Pb$ ratios. The differences between Pb-isotopic signatures of the pyrite types at Sukhoi Log are therefore interpreted to result from differences in either fluid source, fluid–rock interactions along the flow path and/or at the sites of pyrite deposition. Unfortunately, these variables are difficult to constrain particularly as the local geology and the regional Pb isotopic evolution are not well known. The unusual Pb-isotopic compositions of the early stratiform pyrite require the lead to have remained isolated for a significant period in a low Th, high U and Pb environment prior to incorporation into the pyrite. Simple modelling of Pb evolution (Fig. 13) of these rocks indicates a period of isolation of at least 400 m.y. for extremely low Th/U ratios (Th/U = 0.01) and 1000 m.y. for a source with Th/U = 2. Rocks which have low Th/U include carbonates which are slightly lower than typical crustal values (Faure and Mensing, 2005) and some reduced organic-rich black shales which can be strongly enriched in U and Pb compared to Th (e.g. Th/U = 0.01–1: Patterson et al., 1986; Arthur and Sageman,

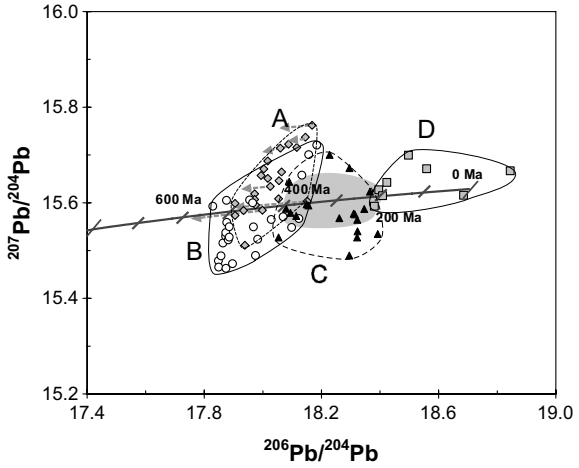


Fig. 11. Laser ablation analyses ICPMS of $^{207}Pb/^{204}Pb$ and $^{206}Pb/^{204}Pb$ in pyrite from the Sukhoi Log deposit. The grey field represents the range of analyses from the Lena Goldfield shown by Larin et al. (1997). The arrows represent position of the early pyrite if a U correction is applied to account for amount of radiogenic Pb generated by the U analysed in the pyrite (see Fig. 12 for more details). Symbols, fields and labels as for Fig. 10.

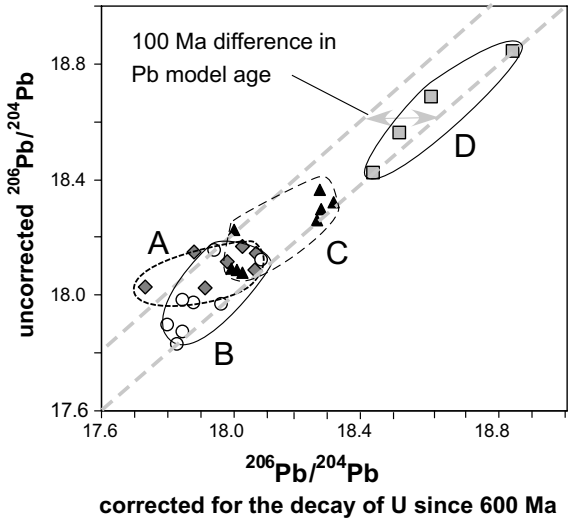


Fig. 12. Comparison of U corrected and uncorrected Pb isotope data. Note that only the quadrupole ICPMS data is shown. The figure show that the decay of the U analysed in the pyrite changes the Pb model ages of the smaller pyrite by 20–100 Ma. Symbols, fields and labels as for Fig. 10.

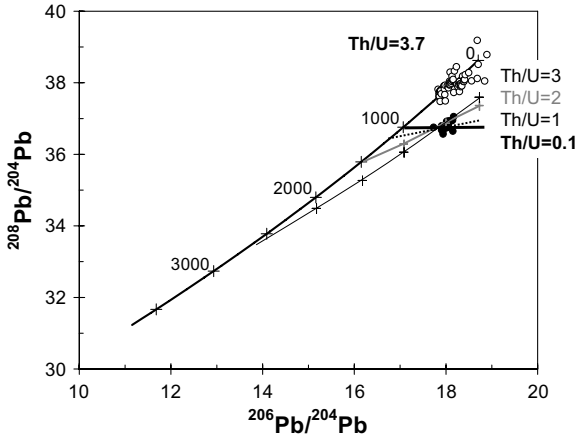


Fig. 13. Pb isotopic models for the formation low $^{208}Pb/^{204}Pb$ in the early stratiform Sukhoi Log pyrite. Uppermost growth curve is from Stacey and Kramers (1975) and shows typical bulk crustal Pb isotopic evolution through time from the early Archean onwards (age in Ma is labelled on curve). The other lines are a family of curves with different Th/U ratios that can be generated from a typical bulk crustal to intersect the low $^{208}Pb/^{204}Pb$ composition of the early stratiform pyrite at 570 Ma. This shows that a reservoir with a low Th/U needs to be separated from crustal Pb sources for at least 400 Ma for the low $^{208}Pb/^{204}Pb$ signature to arise from a normal bulk crustal value at very low Th/U ratio and much longer period of time at lower Th/U values. A possible scenario is that, the Pb in the stratiform pyrite evolved along the upper growth curve up to 1000 Ma, was then incorporated into a low Th/U reservoir and then followed the bold horizontal line to be released and incorporated into the early pyrite at 570 Ma (see discussion for more details).

1994; Coveney, 2000; Algeo and Maynard, 2004). During burial, thick organic-rich black shale successions may produce significant quantities of mobile hydrocarbons, and these have been recently recognised as potentially important agents for the accumulation and transport of many metals, including gold, in sedimentary basins (Emsbo and Koening, 2007; Williams-Jones and Migdisov, 2007). Whilst the apparent paucity of quartz or carbonate veins accompanying the initial stages of gold mineralization at Sukhoi Log may suggest the mineralizing fluids differed from those typically ascribed to the formation of orogenic gold deposits (e.g. Goldfarb et al., 2005), compelling evidence for an influx of deeply-sourced metal-rich hydrocarbons contributing to initial gold enrichment at Sukhoi Log can not yet be demonstrated.

### 4.2. Pb evolution

Whole rock geochemistry indicates that the U/Pb ratios of the sedimentary sequence at Sukhoi Log are typical of upper crustal rocks with average $^{238}U/^{204}Pb = 14$, with a large standard deviation (partial leach average of 57 whole rock analyses from shales and sandstone, standard deviation = 8). Consequently we would expect the Pb isotopic ratios of the host rocks to continue to evolve along the crustal growth curve over time. Pyrite which formed late in the history of the deposit will incorporate some of this radiogenic Pb into its structure, but not U and Th, which are generally excluded from pyrite. This process should produce a more radiogenic Pb-isotopic compositions for pyrite formed later in the paragenetic sequence. The resultant pyrite Pb-model ages, however, are not as precise as U–Pb geochronology, because the common Pb composition of a mineral is determined not by a single decay constant, but by the complex evolution of Pb reservoirs since the Archean. Nevertheless, the Pb isotopic evolution of the pyrite at Sukhoi Log is broadly consistent with constraints provided by dating post-depositional monazite in the host rocks and textural evidence for pyrite growth before, during and after the main deformation and metamorphic event in the Cambrian.

The oldest common Pb-model ages for both the U-corrected stratiform pyrite and the nodular cores to the folded pyrite–quartz veins appear to roughly coincide with growth of low temperature diagenetic (?) monazite cores at ca. 573 Ma, well before peak metamorphism during deformation at ca. 516 Ma. The large euhedral pyrite, and fine-grained sooty and framboidal pyrite have more radiogenic Pb which could indicate either growth at a later time (e.g. during granite intrusion in the Palaeozoic, as suggested by Distler et al. (2004)) or contamination due to the incorporation of radiogenic Pb sourced from the surrounding U-rich sedimentary rocks, or some combination of these processes. Mid to late Palaeozoic ages obtained for some of the small monazites in the wall rocks (i.e. ca. 374 and 288 Ma), suggest the 400–200 Ma Pb-model ages for pyrite comprising Group C (Fig. 10) could be geologically meaningful. However, this pyrite type appears to largely post-date the main phase of gold mineralization at Sukhoi Log (Large et al., 2007)

Evidence for later incorporation of matrix-derived radiogenic Pb is shown by sample 156–225 where the

framboidal pyrite is clearly overgrown by the coarse euhedral pyrite but has a more radiogenic Pb-isotopic composition at broadly similar Pb/U ratios (Fig. 10, see Electronic annex). Due to the small grainsize (i.e. relatively high surface area to volume ratio) of the pyrite crystallites comprising the framboidal and fine-grained sooty pyrite (mostly <1 μm) it is the most likely to undergo significant Pb exchange with the surrounding host rocks late in the history of the deposit, and thus develop an anomalously radiogenic Pb-isotopic signature. Interestingly, this phenomenon does not appear to have affected the texturally similar stratiform fine-grained pyrite, although it has a similar Pb contents. This can be attributed to buffering by the higher lead content of the surrounding rocks, as whole rock geochemical data indicates the main zone of stratiform pyrite in drill hole 1 has much higher lead concentrations (i.e. 40 to >1000 ppm Pb) than other parts of the succession we have analysed (typically 10–40 ppm). Assuming that the lead enrichment in this zone was synchronous with development of the stratiform pyrite, and reflects a similar metal source, the abundance of isotopically similar lead around the stratiform pyrite would effectively mask any subsequent incorporation of radiogenic lead derived from the U-rich shales.

### 4.3. Model for gold deposition and pyrite crystallization

Two possible models for the formation of Sukhoi Log are presented in Fig. 14. These differ from the model presented in Large et al. (2007) in order to take into account some of the new findings of this study.

The earliest stratiform pyrite is thought to have formed from fluids with a distinctive Pb-isotopic composition. The source of the early Pb (and Au) was probably external to the area as the Pb modelling suggests a Th poor, U and Pb rich source at least 400 m.y. older than the immediate host rocks. This Pb was introduced after $600 \pm 10$ Ma but prior to $516 \pm 10$ Ma, during either diagenesis (e.g exhaled from basement or growth faults Fig. 14A) or very early during folding (e.g. possibly discharged from a blind thrust at depth, Fig. 14A′). Although the trace element composition of the early stratiform pyrite suggests the initial mineralizing fluid carried Au as well as Pb (Large et al., 2007), it is impossible to determine what proportion of the total Au at Sukhoi Log may have been ultimately derived from the cryptic low $^{208}$Pb source for the stratiform pyrite in drill hole 1.

Pb-isotopic data for all other pyrite at Sukhoi Log plot along the growth curve suggesting that the Pb, and potentially the Au, were derived from well-mixed crustal sources either in the local sedimentary host rocks or externally. There is no direct Pb-isotopic evidence for recycling of the Pb (and associated Au) that was introduced during the development of the stratiform pyrite (cf. Large et al., 2007). The pyrite which contains the least radiogenic Pb forms the Au-rich cores to folded pyrite–quartz veins along the axial zone of the recumbent anticline. Overprinting relations and Pb-model ages for this pyrite both support growth prior to significant mesoscale folding or cleavage development in the host rocks, and thus prior to, or very early during compressional deformation in the immediate area. Nonetheless, any valid model for the deposit must account for both the distribution of the gold-rich pyrite as well as its apparent timing with respect to meso- and grain-scale deformation features in the host rocks. Both the folded pyrite–quartz veins and their gold-rich nodular pyrite cores are predominantly developed along the axial zone of the anticline, indicating their gross distribution is highly discordant to bedding, and apparently controlled by the geometry of the fold. One explanation, favoured by Large et al. (2007), is that both this early-stage early gold mineralization and subsequent localisation of the anticline were controlled by cross-stratal growth faults active during deposition and subsequent diagenesis of the host sequence (Fig. 14B). Alternately, the gold-rich pyrite nodules could have formed in response to fluid discharge into the axial zone of the fold (possibly above a blind thrust) at a very early stage during fold development (Fig. 14B'). Unfortunately, the data obtained to date do not allow us to clearly differentiate between these competing models for Sukhoi Log. However, we note that both differ from currently favoured orogenic gold models (e.g Groves et al., 2003; Goldfarb et al., 2005), in which gold mineralization is generally thought to have occurred at a relatively late-stage during regional compressional or transpressional deformation.

The large euhedral pyrite (Group C, Fig. 10) which clearly overgrows the axial planar cleavage is more radiogenic than the earlier pyrite consistent with growth late during or after the main folding episode (Fig. 14C). The Pb isotopes suggest timing between 450 and 200 Ma assuming average crustal $^{238}U/^{204}Pb$ ratios (9.7) and up to 50 m.y. earlier assuming upper crustal (or host shale) $^{238}U/^{204}Pb$ ratios (14). Accordingly this pyrite may have formed in the waning stages of the main deformation event in the early Palaeozoic or during the subsequent (late Palaeozoic) intrusion of granites in the region. Although the closest known late Palaeozoic granite is more than 5 km from the deposit, widespread fluid migration at this time (Fig. 14D) is suggested by ca. 374 and 288 Ma ages obtained for some small monazite grains in the host rocks.

The pyrite with the most radiogenic Pb (framboids and patchily-developed fine-grained "sooty" pyrite) is overgrown by (and thus older than) the large euhedral pyrite. This suggesting the Pb-isotopic signature of the non-stratiform fine-grained pyrite was modified post-deposition, by the incorporation of radiogenic Pb sourced from the surrounding U-rich shales. Accordingly this type of pyrite may be similar in age to either that comprising the folded veins or the later coarse euhedral pyrite.

Almost all generations of pyrite crystals at Sukhoi Log contain Au either dissolved in the structure of pyrite, as inclusions of native gold, gold-tellurides or gold-rich galena or along fractures (Large et al., 2007). This indicates either that Au enrichment processes operated over a very long period or as argued by Large et al. (2007), much of the Au was introduced early and was remobilized and concentrated during subsequent metamorphic and/ or magmatic-hydrothermal events.

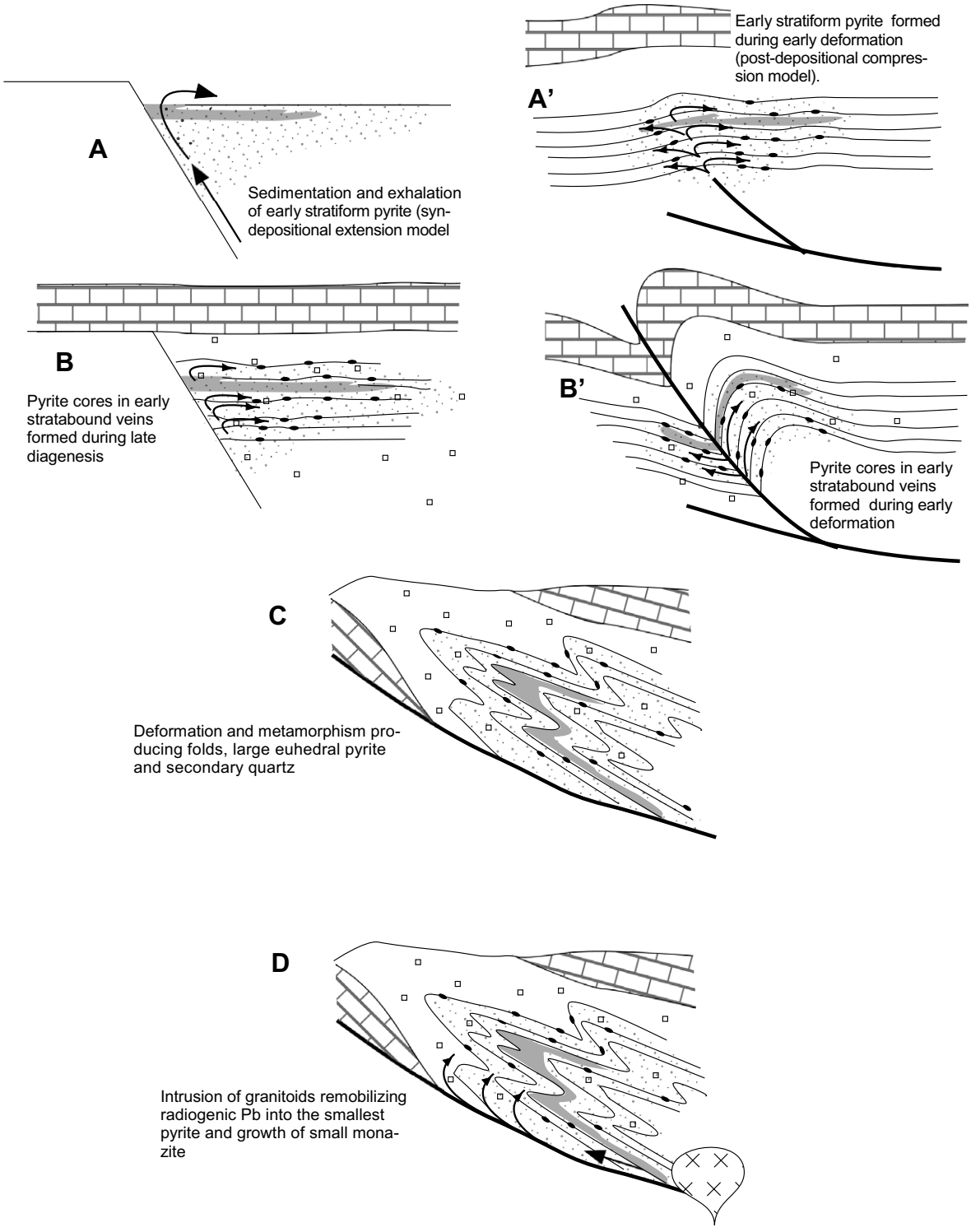


Fig. 14. Paragenetic model for the formation of pyrite at Sukhoi Log showing how each stage relates to a particular Pb-isotopic composition (modified from Large et al., 2007). Symbols as follows: grey area, highest gold enrichment; stippled area, lower gold enrichment; lines, bedding-parallel veins; and squares, carbonate nodules and coarse euhedral pyrite. Capital letters (A–D) refer to pyrite type defined in the text and shown on Figs. 10 and 11.

## 5. CONCLUSION

Pyrite Pb-isotopic compositions, combined with textural observations and U–Th–Pb isotopic dating of detrital zircon and authigenic, metamorphic and hydrothermal monazite at Sukhoi Log, record a protracted history of pyrite formation beginning with pre-deformation growth of Au-bearing (0.2–1.5 ppm) and Pb-rich pyrite during sedimenta-

tion or early diagenesis. Au–Pb-bearing pyrite continued to form throughout Late Neoproterozoic deformation at around 520 Ma and during subsequent metamorphic/hydrothermal events in the Palaeozoic. Most of the Pb plots close to bulk crustal growth curves suggesting well-mixed crustal metal sources, however, early stratiform pyrite contains Pb derived from a source characterised by low Th/U and Th/Pb ratios suggesting ultimate derivation from much older organic-rich shales and a possible hydrocarbon-linked metal transport process.

## ACKNOWLEDGMENTS

This research was supported by funding from the Australian Research Council Centre of Excellence grant to R.R.L. Thanks to Vladimir Martynyuk, Valery Benedyk and Ekaterina Evlapova for providing samples for this study. Thanks also to Ron Berry for help with monazite chemistry and Karsten Goemann for help with the electron microprobe work. This paper has benefitted from thorough and constructive reviews by Richard Tosdal, Bruce Eglington and Richard Herrington.

## APPENDIX A. SUPPLEMENTARY DATA

Pb, U and Th isotopic and trace element data for Sukhoi Log pyrite, zircon and monazite. Supplementary data associated with this article can be found, in the online version, at doi:10.1016/j.gca.2008.03.005.

## REFERENCES

Algeo T. J. and Maynard J. B. (2004) Trace-element behavior and redox facies in core shales of Upper Pennsylvanian Kansas-type cyclotherms. *Chemical Geology* **206**, 289–318.

Arthur M. A. and Sageman B. B. (1994) Marine black shales: depositional mechanisms and environments of ancient deposits. *Annual Review of Earth & Planetary Sciences* **22**, 499–551.

Berry R. F., Chmielowsky R. M., Steele D. A. and Meffre S. (2007) Chemical U–Th–Pb dating of the Cambrian Tyennan Orogeny, Tasmania. *Australian Journal of Earth Sciences* **54**, 761–775.

Black L. P., Kamo S. L., Allen C. M., Aleinikoff J. N., Davis D. W., Korsch R. J. and Foudoulis C. (2003) TEMORA 1: a new zircon standard for Phanerozoic U–Pb geochronology. *Chemical Geology* **200**, 155–170.

Black L. P., Kamo S. L., Allen C. M., Davis D. W., Aleinikoff J. N., Valley J. W., Mundil R., Campbell I. H., Korsch R. J., Williams I. S. and Foudoulis C. (2004) Improved $^{206}Pb/^{238}U$ microprobe geochronology by the monitoring of a trace-element related matrix effect; SHRIMP, ID-TIMS, ELA-ICP-MS, and oxygen isotope documentation for a series of zircon standards. *Chemical Geology* **205**, 115–140.

Buryak V. A. (1982) *Metamorphism and Ore Formation*. Nedra Press, Moscow.

Compston W. (1999) Geological age by instrumental analysis: the 29th Hallimond Lecture. *Mineralogical Magazine* **63**, 297–311.

Coveney R. M. (2000) Roles of organic matter in black shale- and carbonate-hosted base metal deposits. In *Ore Genesis and Exploration: The Roles of Organic Matter* (eds. T. H. Giordano, R. M. Kettler and S. A. Wood). *Reviews in Economic Geology*, vol. 9, pp. 251–274.

Distler V. V., Yudovskaya M. A., Mitrofanov G. L., Prokof'ev V. Y. and Lishnevskii E. N. (2004) Geology, composition, and genesis of the Sukhoi Log noble metals deposit, Russia. *Ore Geology Reviews* **24**, 7–44.

Emsbo P., Hutchinson R. W., Hofstra A. H., Volk J. A., Bettles K. H., Baschuk G. J. and Johnson C. A. (1999) Syngenetic Au on the Carlin Trend; implications for Carlin-type deposits. *Geology* **27**, 59–62.

Emsbo P., Groves D., Hofstra A. and Bierlein F. (2006) The giant Carlin gold province: a protracted interplay of orogenic, basinal, and hydrothermal processes above a lithospheric boundary. *Mineralium Deposita* **41**, 517–525.

Emsbo P. and Koening A. E. (2007) Transport of Au in petroleum: evidence from the northern Carlin Trend, Nevada. In *Proceedings of the Ninth Biennial SGA Meeting*, Dublin, pp. 695–698.

Faure G. and Mensing M. T. (2005) *Isotopes: Principles and Applications*. Wiley.

Fefelov N. N., Sharov V. N. and Yablonovskii B. V. (2000) Pb–Pb age of metamorphosed carbonate deposits of the Imnyakh Formation (Bodaibo synclinorium). *Geologiya I Geofizika* **41**, 86–89.

Foster G., Gibson H. D., Parrish R., Horstwood M., Fraser J. and Tindle A. (2002) Textural, chemical and isotopic insights into the nature and behaviour of metamorphic monazite. *Chemical Geology* **191**(1–3), 183–207.

Goldfarb R. J., Baker T., Dubé B., Groves D. I., Hart C. J. R. and Gosselin P. (2005) Distribution, character, and genesis of gold deposits in metamorphic terranes. In *Economic Geology and the Bulletin of the Society of Economic Geologists, One Hundredth Anniversary Volume 1905–2005* (eds. J. W. Hedenquist, J. F. H. Thompson, R. J. Goldfarb and J. P. Richards), pp. 407–450.

Groves D. I., Goldfarb R. J., Robert F. and Hart C. J. R. (2003) Gold deposits in metamorphic belts: overview of current understanding, outstanding problems, future research, and exploration significance. *Economic Geology and the Bulletin of the Society of Economic Geologists* **98**, 1–29.

Hand M., Mawby J., Kinny P. and Foden J. (1999) U–Pb ages from the Harts Range, central Australia: evidence for early Ordovician extension and constraints on Carboniferous metamorphism. *Journal of the Geological Society* **156**, 715–730.

Heinrich W., Andrehs G. and Franz G. (1997) Monazite–xenotime miscibility gap thermometry. 1. An empirical calibration. *Journal of Metamorphic Geology* **15**, 3–16.

Jackson S. E., Pearson N. J., Griffin W. L. and Belousova E. A. (2004) The application of laser ablation-inductively coupled plasma-mass spectrometry to in situ U–Pb zircon geochronology. *Chemical Geology* **211**, 47–69.

Kosler J. and Sylvester P. J. (2003) Present trends and the future of zircon in geochronology; laser ablation ICPMS. *Reviews in Mineralogy and Geochemistry* **53**, 243–275.

Kuz'min M. I., Yarmolyuk V. V., Spiridonov A. I., Nemerov V. K., Ivanov A. I. and Mitrofanov G. L. (2006) Geodynamic setting of gold ore deposits of the Neoproterozoic Bodaibo trough. *Doklady Earth Sciences* **407**, 397–400.

Large R. R., Maslennikov V. V., Robert F., Danyushevsky L. V., Scott R. J. and Chang Z. (2007) Multi-stage sedimentary and metamorphic origin of pyrite and gold in the Giant Sukhoi Log deposit, Lena Goldfield, Russia. *Economic Geology* **102**(7).

Larin A. M., Rytsk Y. Y. and Sokolov Y. M. (1997) Baikal-Patom fold belt. In *Precambrian Ore Deposits of the East European and Siberian Cratons* (eds. D. V. Rundqvist and C. Gillen). Elsevier, pp. 317–379.

Ludwig K. R. (2003) User Manual for Isoplot 3.0. *Berkeley Geochronology Center Special Publication* **4**, Berkeley, USA.

Machado N. and Gauthier G. (1996) Determination of $Pb^{207}/Pb^{206}$ ages on zircon and monazite by laser-ablation ICPMS and application to a study of sedimentary provenance and meta-

morphism in southeastern Brazil. *Geochimica et Cosmochimica Acta* **60**, 5063–5073.

Meffre S., Scott R. J., Glen R. A. and Squire R. J. (2007) Re-evaluation of contact relationships between Ordovician volcanic belts and the quartz-rich turbidites of the Lachlan Orogen. *Australian Journal of Earth Sciences* **54**, 363–383.

Montel J.-M., Foret S., Veschambre M., Nicollet C. and Provost A. (1996) Electron microprobe dating of monazite. *Chemical Geology* **131**, 37–53.

Patterson J. H., Ramsden A. R., Dale L. S. and Fardy J. J. (1986) Geochemistry and mineralogical residences of trace elements in oil shales from Julia Creek, Queensland, Australia. *Chemical Geology* **55**, 1–16.

Rubatto D., Williams I. S. and Buick I. S. (2001) Zircon and monazite response to prograde metamorphism in the Reynolds Range, central Australia. *Contributions to Mineralogy and Petrology* **140**, 458–468.

Schandl E. S. and Gorton M. P. (2004) A textural and geochemical guide to the identification of hydrothermal monazite: criteria for selection of samples for dating epigenetic hydrothermal ore deposits. *Economic Geology and the Bulletin of the Society of Economic Geologists* **99**, 1027–1035.

Stacey J. S. and Kramers J. D. (1975) Approximation of terrestrial lead isotope evolution by a two-stage model. *Earth and Planetary Science Letters* **26**, 207–221.

Sun S.-S. and McDonough W. F. (1989) Chemical and isotopic systematics of oceanic basalts: implications for mantle composition and processes. In *Magmatism in the Ocean Basin* (eds. A. D. Saunders and M. J. Norry), vol. 42, pp. 313–345.

Wiedenbeck M., Alle P., Corfu F., Griffin W. L., Meier M., Oberli F., Vonquadt A., Roddick J. C. and Speigel W. (1995) 3 Natural zircon standards for U–Th–Pb, Lu–Hf, trace-element and Ree analyses. *Geostandards Newsletter* **19**, 1–23.

Williams-Jones A. E. and Migdisov A. A. (2007) The solubility of gold in crude oil: implications for ore genesis. In *Proceedings of the Ninth Biennial SGA Meeting*, Dublin, pp. 765–768.

Wood B. L. and Popov N. P. (2006) The giant Sukhoi Log gold deposit, Siberia. *Russian Geology and Geophysics* **47**, 317–341.

Woodhead J. D. (2002) A simple method for obtaining highly accurate Pb isotope data by MC-ICP-MS. *Journal of Analytical Atomic Spectrometry* **17**, 1381–1385.

*Associate editor:* Edward M. Ripley